1516
doi:10.1017/S1431927618008061
Microsc. Microanal. 24 (Suppl 1), 2018

In-situ Probe of Lithium-ion Transport and Phase Evolution Within and Between Silver Hollandite Nanorods

Lijun Wu[1], Feng Xu[1,2], Qingping Meng[1], Amy C. Marschilok[3], Esther S. Takeuchi[3], Kenneth J. Takeuchi[3], Mark S. Hybertsen[4] and Yimei Zhu[1]

[1.] Department of Condensed Matter Physics & Materials Science, Brookhaven National Laboratory, Upton, USA.
[2.] Key Laboratory of MEMS of the Ministry of Education, Southeast University, Nanjing, China.
[3.] Department of Chemistry, Stony Brook University, Stony Brook, USA.
[4.] Center for Functional Nanomaterials, Brookhaven National Laboratory, Upton, USA.

Porous manganese oxides such as Ag doped α-MnO_2 hollandites have gained significant attentions as electroactive materials as their tunnel-based crystallographic structure may provide sufficient structural rigidity to enable repeated ion exchange within their one-dimensional forms [1]. Specifically, hollandite type materials consist of edge-sharing MnO_6 octahedra which interlink to form tunnels (Fig. 1n). Using an in situ TEM approach (Fig. 1a), lithiation of $Ag_{1.6}Mn_8O_{16}$ nanorods was observed in 'operando', revealing Li^+ diffusion in individual nanorods not only along their longitudinal (or tunnel) direction, but also in the lateral (a-b plane) direction between the nanorods. As shown in Fig. 1, upon applying the electrostatic potential, we observed changes in the interior contrast of nanorod I where many needle-like regions (β-region) became visible (Fig. 1c–e). After 3s, a distinct lithiation reaction front (RF) appeared and propagated longitudinally, Fig. 1f–k, while the region (γ-region) characterized by numerous tiny crystallites behind it underwent a 27.6% radial expansion. Comparing EELS measurement of the chemically lithiated reference samples, we estimated that the β- and γ- regions correspond to ~0.9 Li^+ and >6 Li^+ equivalent, respectively (Fig. 1o). After ~24 s, the RF from nanorod I reached nanorod II where a second pathway for lithium transport was observed. At 34 s, the RF has crossed the boundary between the two rods and formed a reacted area centered at the top part of nanorod II (Fig. 1j). The RF reached the bottom edge of the nanorod II at 42 s (Fig. 1k). It also continued to propagate along the c axis of nanorod II. Our observations reveal the lithiation proceeded in both directions, away from the point of contact with nanorod I. Analysis of the RF progress in nanorod II indicated an estimated velocity of 1.9 nm/s across the diameter of the rod and a velocity of ~4.4 nm/s longitudinally, indicating an asymmetry for RF motion in the a-b direction and along the c axis. Starting at ~42 s, the lateral and longitudinal lithium transport pathways were observed simultaneously for nanorod III [2].

To provide insight into the observed lithiation dynamics, we conducted density function theory (DFT) and phase-field model calculations. Starting from an initial state of uniform Li concentration x~0.7 (Fig. 2c), subsequent lithiation led to a phase separation with co-existence of Ag-rich/Li-free (x~0, β_1) and Li-poor (x~1, β_2) phases (Fig. 2d). As lithiation continued, the high Li concentration (x~8, γ-phase) nucleated and grew from the electrolyte/electrode interface (Fig. 2e). At the same time the coarsening of β_1+β_2 continued slowly. The evolution of β_1 and β_2 largely depends on the energy barrier between the two phases. The simulations exhibit the balance between the time scale associated to the RF motion and the β_1-phase coarsening, consistent with the experimental observations shown in Fig. 1 [3].

References:

[1] S. L. Brock *et al*, Chem. Mater. **10**, 2619–2628 (1998).
[2] Feng Xu *et al*, Nature Communications **8** (2017).

[3] This work was supported by the US DOE-BES, MSE Division under Contract No. DESC0012704 and the Center for Mesoscale Transport Properties under award #DE-SC0012673.

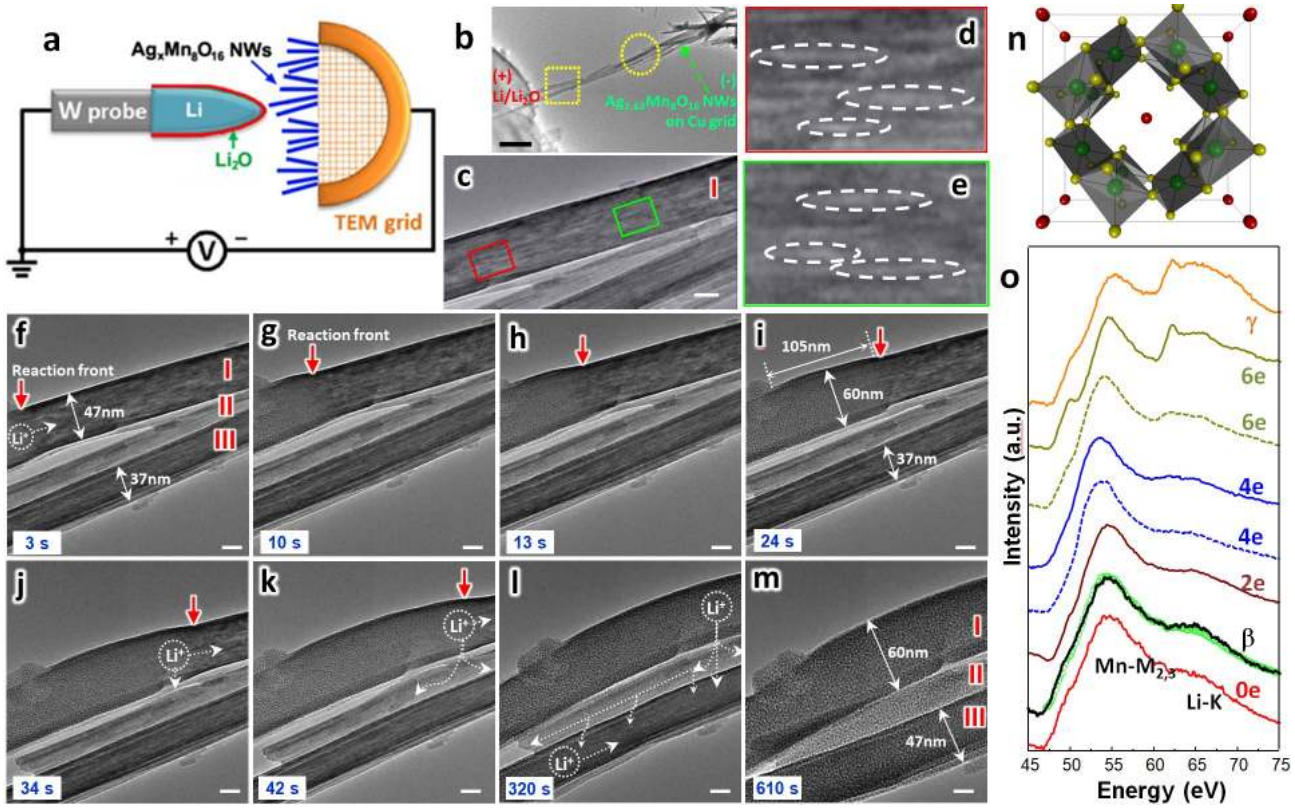

Figure 1. (a) Schematic illustration of the experiment setup. Electrochemical lithiation was initiated by applying a constant potential of -1.0V to the nanorods with respect to the Li counter electrode. (b) The panoramic image of the region with Li/Li_2O on the left. Scale bar, 500 nm. (c–m) Snapshots of the lithiation process from video, showing the three types of Li-transport pathways for three nanorods (I-III) in the boxed area in b. Scale bars, 20 nm. (d,e) Magnified images from the red and green boxed area in c, showing the early stage of lithiation with needle-like domains. (n) Structure model with green, yellow and red spheres representing Mn, O and Ag, respectively. (o) EELS from ex-situ chemical lithiated (0e-6e equivalent) and in situ TEM-lithiated samples. The Li-K edges from β- and γ-regions are compared with those from chemical lithiated samples (0e-6e), revealing the Li concentration in the β-region is about 0.9e equivalent, while the γ-region is more than 6e equivalent.

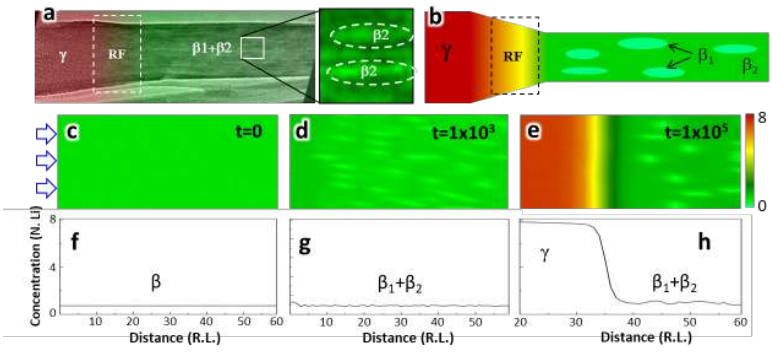

Figure 2. (a) An experimental snap shot from the in situ TEM observation, showing three distinct regions: the lithiation RF, the area in front of the RF (β1+β2), and behind (γ). (b) Schematic of the co-existing phases in (a). (c-e) Snapshots from two-dimensional phase-field simulations illustrating dynamical evolution of the microstructure for three instants of time. The top row shows two-dimensional maps with the color legend indicating normalized Li concentration and the bottom row shows one dimensional Li-concentration as a function of distance.

https://doi.org/10.1017/S1431927618008061 Published online by Cambridge University Press